THE JOURNAL OF PHYSICAL CHEMISTRY C

ARTICLE

pubs.acs.org/JPCC

Structures and Energetics of Silver and Gold Nanoparticles

Boyang Wang, Maoxin Liu, Yanting Wang,* and Xiaosong Chen

Key Laboratory of Frontiers in Theoretical Physics, Institute of Theoretical Physics, Chinese Academy of Sciences, 55 Zhongguancun East Road, Beijing 100190, P. R. China

ABSTRACT: The stability and energetics of metal nanoparticles are very important for their wide applications. Ino developed a continuous model combined with experimental parameters to study the stability of metal nanoparticles for several different crystalline structures. To provide comparable information for molecular simulation results, we re-examined Ino's theory by using the parameters of the Sutton−Chen potential for silver and gold, respectively. Our results show that the most stable structure is icosahedron when the diameter is smaller than 2 nm, and truncated octahedron for larger nanoparticles. Static energies were then calculated for perfect crystalline structures to compare with the results by Ino's theory, and different crystalline stabilities have been found. Nevertheless, all calculations indicate that truncated octahedron is the most stable structure at large sizes. Finally, thermodynamic effects have been demonstrated to be non-negligible by finding the thermodynamically stable structures of metal nanoparticles with the simulated annealing method. Therefore, experimentally developed metal nanoparticles do not necessarily always take the structure with the lowest potential energy given by either Ino's theory or static energy calculations.

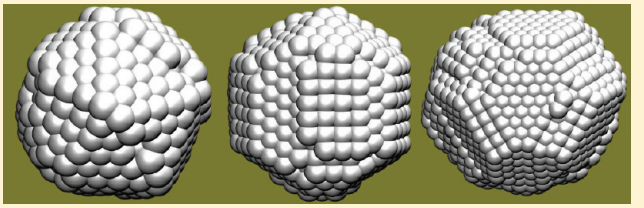

1. INTRODUCTION

Over the past two decades, nanomaterials, such as nanoparticles,[1] nanorods,[2] nanowires,[3] and carbon nanotubes,[4] have been studied extensively in both basic research and industrial applications. Specifically, nanoparticles have drawn lots of attention, due to their better physical and chemical homogeneity as compared to their bulk counterparts.[5,6] Nanoparticles are chemically active and can be used as catalysts,[7] biomarkers when being linked to proteins,[8] and drug carriers inside cells.[9] Nanoparticles could also be integrated in the design of nanomachines in the future.[10−12] Metal nanoparticles, especially those with small sizes, are catalytically very active and selective when they are dispersed in supporting matrices.[7,13−20] Thin films of semiconducting nanoparticles are used as materials for electronic and optoelectronic devices such as field-effect transistors,[21−27] photodetectors,[28−31] light-emitting diodes,[32−36] metamaterials,[37−39] and solar cells.[40,41] Nanoparticles also have very wide applications in building nanocomposite materials[42−48] due to their better mechanical and optical properties. The thermodynamics and structures of nanoparticles are crucial for their functionalities, because structural transformation of nanoparticles[49] influences their electronic and optical properties,[50] changes their sintering kinetics,[51,52] and further controls the catalytic activities of nanoparticles.[53,54] Therefore, theoretical studies of the structures and energetics of nanoparticles are very important for supporting their wide applications.

Predicting the equilibrium shape of a crystal can be based on the Wulff construction, which requires minimization of surface free energy of the crystal for a given enclosed volume.[55] Ino[56] first applied this approach to several metal and nonmetal nanoparticles by calculating the total internal energy of tetrahedral, octahedral, truncated octahedral, icosahedral, decahedral, and truncated decahedral (Ino decahedral) structures with the macroscopic quantities of cohesive, surface, twin-boundary, and elastic strain energies. All the truncated motifs are optimal ones from the Wulff construction. The parameters for those energy terms were obtained from fitting the experimentally measured properties. Ino found that metal and nonmetal nanoparticles (Ag, Au, Al, Cu, Ge, Ni, Pb, Pd, Pt, Si, β-Co, γ-Fe) with a diameter smaller than about 10 nm prefer to have an icosahedral structure, and those with larger diameters prefer to be truncated octahedron. More recently, Marks[57,58] proposed a modification to the Ino decahedral structure, termed "Marks decahedron", which includes concave facets at the twin boundaries of the Ino decahedron. The Marks decahedron was found to be the most preferable structure in an intermediate size region between icosahedron and truncated octahedron, later confirmed by Baletto et al.[59,60] There have been plenty of computational studies on the structures of gold nanocrystals, by either *ab initio*[61−70] or molecular dynamics (MD) methods.[71−76] However, all these studies have focused on gold nanoparticles with a number of atoms $N < 500$ (diameter of about 2.5 nm), in many cases much smaller than the usual experimentally prepared nanoparticles. It is also unclear from previous studies how thermodynamic effects can influence the structure of nanoparticles. Therefore, more systematic studies are needed for testing the validity of traditional theories in these systems, for studying the structures and energetics of larger nanoparticles, and also for studying the influence of thermodynamic effects on the stability of nanoparticles.

Received: January 31, 2011
Revised: May 4, 2011
Published: May 20, 2011

dx.doi.org/10.1021/jp201023x | *J. Phys. Chem. C* 2011, 115, 11374–11381

Among several widely used computational methods,[77] such as *ab initio* calculation, classical MD simulation, and energy minimization, with the current computer power, MD simulation and energy minimization are the two methods that can be applied to study large nanoparticles with a size of about $N > 1000$. Both methods require the use of empirical atomistic force fields, so Ino's results[56] with the parameters obtained from experiments are not directly applicable to interpreting and understanding simulation results. Therefore, in this study, we re-explored Ino's analytical theory by obtaining the parameters from empirical force fields for silver and gold nanoparticles, respectively. Our results qualitatively agree with Ino's results that the icosahedral structure is the most stable in the small size region and the truncated octahedron is the most stable in the large size region. However, the transition point shifts to a diameter ~2 nm, much smaller than ~10 nm given by Ino's original calculations.[56]

To estimate the errors of the analytical model, nanoparticles with various structures were manually constructed and minimized by the energy minimization method, and their internal energies were then calculated and compared with those given by the analytical calculations with Ino's theory. The calculations demonstrated more complicated stability behavior of gold and silver nanoparticles. Nevertheless, all calculations indicate that truncated octahedron is the most stable structure at large sizes.

Both analytical and energy minimization methods study the stability of nanoparticles only by comparing the internal energies of different structures without considering dynamic process and entropy contribution at a finite temperature. To illustrate how important thermodynamic effects are to the structure of metal nanoparticles, we quenched the Ag and Au nanoparticles from liquid to solid by employing the simulated annealing computational method.[78] The results indicate that the thermodynamic effect is non-negligible in determining the stable structure of metal nanoparticles.

2. ANALYTICAL CALCULATIONS WITH INO'S THEORY

Ino's theory[56] originally used experimental parameters, such as elastic strain energies and surface energies, of different types of metals, to analytically calculate the stability of different structures of nanoparticles. Computational methods with specific empirical force fields, such as the Sutton−Chen force field,[79] the embedded atom method,[80] and the glue model,[81] have been developed to predict properties of metals, such as melting point and elastic strain energies. In order to make direct comparison with simulation rather than experimental results, we re-explored Ino's formalism applying to Ag and Au nanoparticles by using the parameters determined from the Sutton−Chen force field.

The stability of a nanoparticle's crystal structure is the balance of three energetic factors: the total surface energy, the total elastic strain energy, and the total twin boundary energy. According to Ino's theory,[56] the total internal energy, U_n for a uniformly structured particle and U_m for a multiply twinned one, respectively, are expressed as

$$\begin{aligned} U_n &= -U_c + U_s \\ U_m &= -U_c + U_s + U_e + U_t \end{aligned} \quad (1)$$

where U_c, U_s, U_e, and U_t are the cohesive energy, the surface energy, the elastic strain energy, and the twin boundary energy, respectively, and

$$\begin{aligned} U_c &= VE_c \\ U_s &= S_{111}\gamma_{111} + S_{100}\gamma_{100} \\ U_e &= VW \\ U_t &= T\gamma_t \end{aligned} \quad (2)$$

where V is the crystal volume and E_c is the cohesive energy per unit volume. S_{111} and S_{100} are the surface areas of (111) and (100) facets, respectively. γ_{111} and γ_{100} are the surface energy in a unit area of (111) and (100) facets, respectively (only these two kinds of facets are present in the crystal structures we study). W is the elastic strain energy per unit volume, T is the total twin boundary area, and γ_t is the twin-boundary energy in a unit area. The icosahedral, decahedral, and truncated decahedral structures all have elastic strain energy and twin boundary energy.

Since the cohesive energy E_c is the same for different structures, the stability of a nanoparticle results from the competition between the surface energy term and the elastic strain energy term. The minimization of the surface energy can be achieved by keeping the total surface area minimal and the surface mostly covered by the closely packed (111) facets. The shape of icosahedron is the closest to a sphere in all polyhedra, so it has the smallest surface area. It is also totally covered by (111) facets, which allows it to be the most stable structure at small sizes. However, its elastic strain energy increases quickly with volume, so it is not preferred at large sizes. Both decahedral and truncated decahedral structures also have elastic strain energies. Although the shape of truncated decahedron is a little closer to a sphere than decahedron, the truncation exposes some (100) facets, whose surface energy is higher than (111) facets. These two structures are unstable at large sizes, also because the elastic strain energies increase quickly with volume. The tetrahedral and octahedral structures both have no elastic strain energy, and are totally covered by (111) facets, but their surface area are very large. The truncated octahedral structure is partly covered by (100) facets, but it has less surface area than tetrahedral and octahedral structures. The stability of nanocrystal structure is the result of a subtle balance between those energetic factors, and they are calculated below.

The experimental value of γ_t[56] was used in this study, since it is very small and almost does not participate in determining the most stable structure. The energy minimization was used to evaluate the coefficients, E_c, γ_{111}, γ_{100}, and W for icosahedral, decahedral, and truncated decahedral structures. The DL_POLY software package[82] was employed to perform the energy minimization for Au and Ag nanoparticles with the Sutton−Chen many-body force field.[79] To calculate the cohesive energies E_c, 3072 silver or gold atoms were arranged as 32 layers with an fcc lattice structure. Experimental lattice constants of 4.090 and 4.080 Å were used for silver and gold, respectively. Periodic boundary conditions were applied to mimic the bulk material of silver or gold. Energy minimization was performed to obtain the lowest energy of the system. The cohesive energy density E_c was then calculated by dividing the total energy by the number of atoms. The surface energy density coefficients γ_{111} and γ_{100} were calculated with the procedure described below. There were 64 Ag (Au) (111) ((100)) planar layers generated with a surface area S_{111} (S_{100}). The periodic boundary conditions were applied to mimic an infinitely large slab of surface. Energy minimization was performed to obtain the lowest energy of this system, noted as

Table 1. Cohesive Energies E_c, Surface Energy Density Coefficients γ, and Strain Energy Density Coefficients W Estimated by the Energy Minimization Method Compared with the Experimental Values

	minimized	experimental[56]
E_{c-Ag} (eV/atom)	2.958	2.96
E_{c-Au} (eV/atom)	3.780	3.78
γ_{100-Ag} (J/m^2)	1.018	1.738
γ_{111-Ag} (J/m^2)	1.000	1.505
γ_{100-Au} (J/m^2)	0.619	2.271
γ_{111-Au} (J/m^2)	0.549	1.967
W_{i-Ag} (10^8 J/m^3)	1.850	1.669
W_{d-Ag} (10^8 J/m^3)	0.734	0.126
W_{i-Au} (10^8 J/m^3)	5.300	1.531
W_{d-Ag} (10^8 J/m^3)	0.336	0.121

E_{64}. The same procedure was also applied to a surface slab with 128 layers to obtain an minimized energy of E_{128}. The surface energy density of (111) was then calculated by $\gamma_{111} = (E_{64} - {}^1/_2E_{128})/S_{111}$.

To determine the strain energy density W, we first applied the energy minimization to a perfectly structured 2869-atom icosahedron and an 835-atom decahedron. A 165-atom tetrahedral unit was carved out from both structures with an internal energy of E_{tetra}. This tetrahedron was then relaxed to obtain the relaxed internal energy E_{relax}. The strain energy density of icosahedron was calculated by $W = (E_{tetra} - E_{relax})/V_{tetra}$, where V_{tetra} is the volume of this tetrahedron. The same procedure was also applied to a 835-atom decahedron. Our calculations with other icosahedra and decahedra (data not shown) demonstrate that W does not change much with system size in the small size region. The calculated values of E_c, γ_{111}, γ_{100}, and W are listed in Table 1, compared with the experimental values,[56] in which the strain energy density coefficients for the icosahedral and decahedral structures are denoted as W_i and W_d, respectively. We can see from this table that our E_c values are almost identical with the experimental values. The γ_{111} and γ_{100} values estimated by our energy minimization are significantly smaller than the experimental values, while the W values estimated by the energy minimization are mostly much higher than the experimental values. This discrepancy might mainly come from the approximations built in the Sutton−Chen force field.

The coefficients determined with the Sutton−Chen potential were put in Ino's formula, eqs 1 and 2, to analytically calculate the internal energy for different structures. The average internal energies per atom versus numbers of atoms are plotted in lines for Ag in Figure 1 and Au in Figure 2. As shown in Figure 1, for Ag nanoparticles, the icosahedral structure has the lowest energy for $N < 300$, and the truncated octahedral structure is the lowest for $N > 300$. For Au nanoparticles, as shown in Figure 2, icosahedron has the lowest energy for $N < 200$, and truncated octahedron has the lowest energy for $N > 200$. These transition points correspond to a diameter ~2 nm, much smaller than ~10 nm of Ino's original calculations.

3. ENERGY MINIMIZATION FOR CONSTRUCTED PERFECT STRUCTURES

The above method based on Ino's theory assumes that the internal energy of a cluster is composed of cohesive, surface, elastic strain, and twin boundary energies, and it changes continuously with system size. The advantage of this method is that it can be used to calculate the energy of a cluster with an arbitrary large size. On the other hand, the approximations made in its continuity and energy terms inevitably cause some errors, which can be justified by explicitly calculating the internal energies of

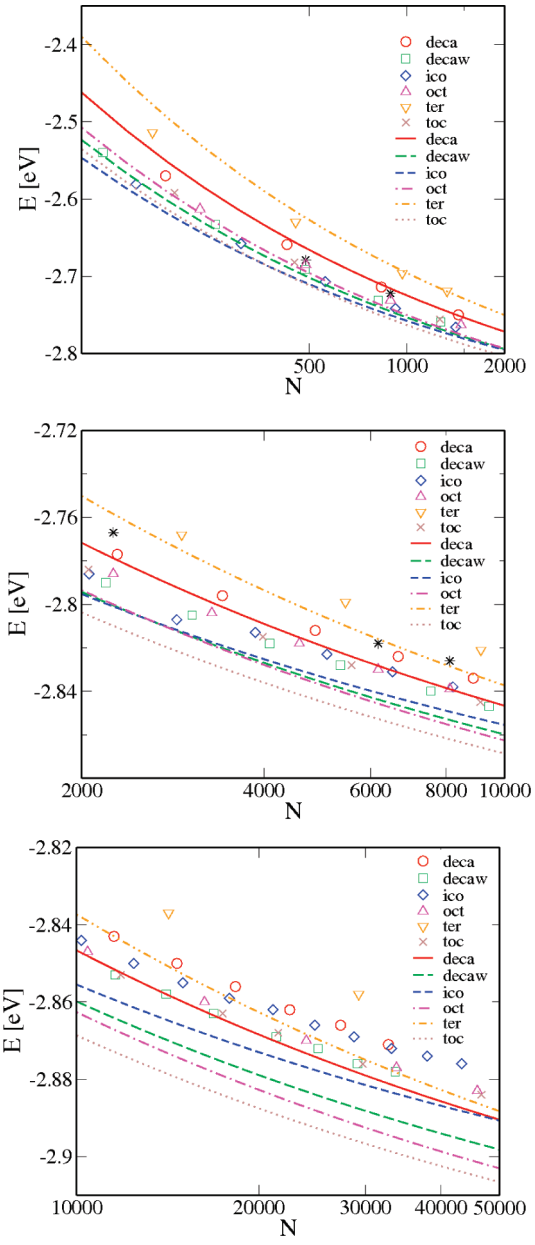

Figure 1. Average potential energies per atom for different structures of Ag nanoparticles with $N < 2000$ (top), $2000 < N < 10\,000$ (middle), and $10\,000 < N < 50\,000$ (bottom), calculated with the Sutton−Chen potential. Analytical results calculated with Ino's theory are plotted in lines: red solid, decahedron (deca); green dashed, truncated decahedron (decaw); blue short dashed, icosahedron (ico); magenta dot dashed, octahedron (oct); orange double dot dashed, tetrahedron (ter); gray dot, truncated octahedron (toc). Those for perfect structures are shown in symbols: circle, decahedron; square, truncated decahedron; diamond, icosahedron; triangle up, octahedron; triangle down, tetrahedron; cross, truncated octahedron. Potential energies per atom at $T = 100$ K after simulated annealing are shown in black stars.

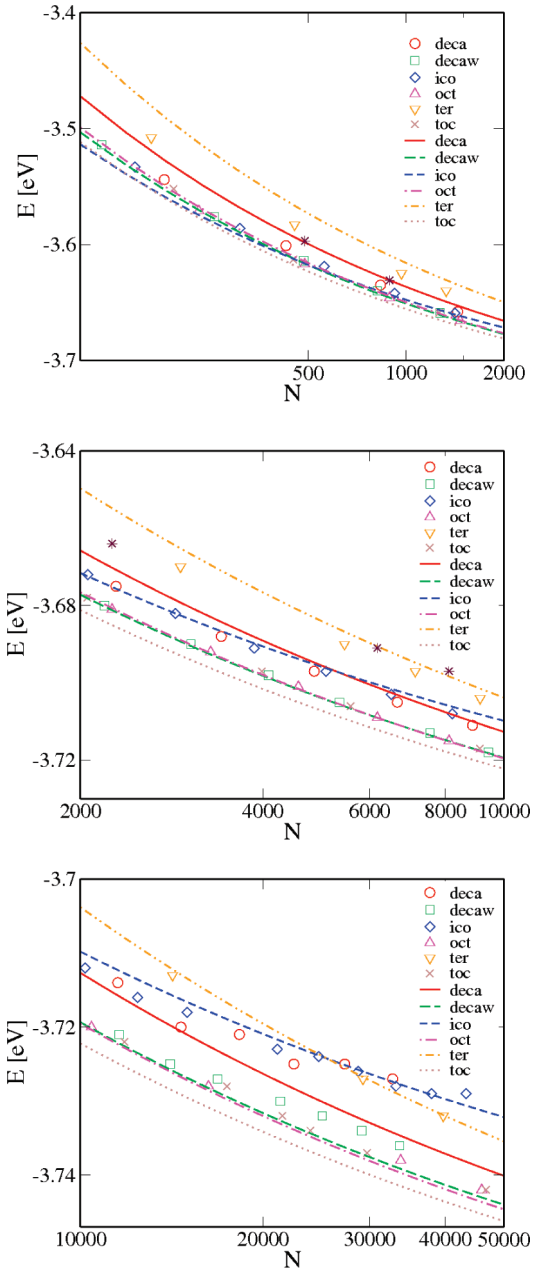

Figure 2. Average potential energies for different structures of Au nanoparticles with $N < 2000$ (top), $2000 < N < 10\,000$ (middle), and $10\,000 < N < 50\,000$ (bottom), calculated with the Sutton−Chen potential. The legends are the same as in Figure 1.

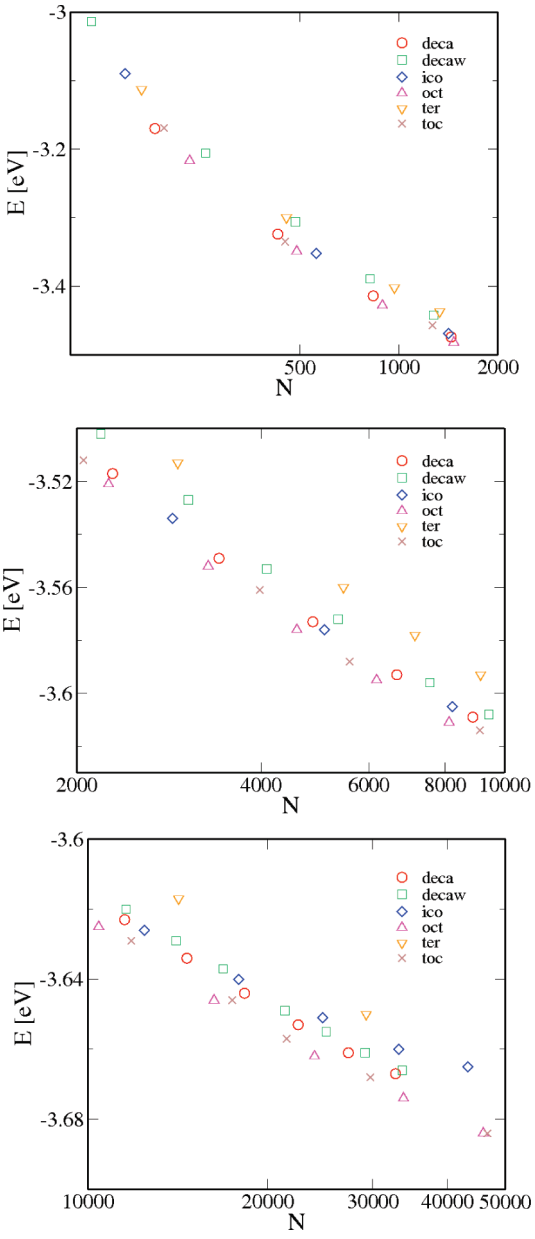

Figure 3. Minimized energies of different structures of Au nanoparticles with $N < 2000$ (up), $2000 < N < 10\,000$ (middle), and $10\,000 < N < 50\,000$ (bottom), calculated with the glue model. The legends are the same as in Figure 1.

individual clusters with the same interaction model. Energy minimization was categorized by Barnard[77] as one of the major computational methods for simulating nanoparticles. To evaluate the errors made in the analytical calculations with Ino's theory, we manually constructed the Ag and Au nanoparticles with perfect tetrahedral, octahedral, icosahedral, decahedral, truncated octahedral, and truncated decahedral structures. The energy minimizations were performed with the DL_POLY software package,[82] using the Sutton−Chen many-body force field.[79] The results are plotted in Figure 1.

For Ag nanoparticles, as shown in the top panel of Figure 1, the minimized energy of icosahedron is the lowest for $N < 2000$, but very close to the minimized energies of truncated decahedron, truncated octahedron, and octahedron. Decahedron has a higher energy, and tetrahedron has the highest. In the middle panel of Figure 1, icosahedron still has the lowest energy for $N < 3000$, but truncated decahedron becomes the lowest for $3000 < N < 10\,000$. The minimized energies of truncated decahedron and truncated octahedron are very close to each other in the size range $2000 < N < 10\,000$. The minimized energies of the icosahedral and octahedral structures are also very close at $3000 < N < 10\,000$. The minimized energy of the decahedral structure is higher, and that of the tetrahedral structure is the highest. In the bottom panel of Figure 1, truncated decahedron has the lowest energy for $10\,000 < N < 30\,000$, and truncated octahedron becomes lowest for $N > 30\,000$. The minimized energy of octahedron is higher than

dx.doi.org/10.1021/jp201023x |J. Phys. Chem. C 2011, 115, 11374–11381

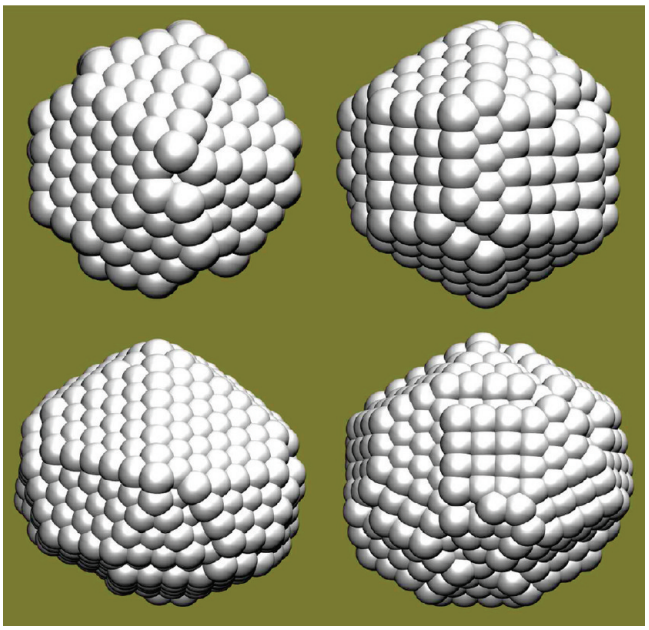

Figure 4. Truncated decahedral structures of Ag nanoparticles obtained for $N = 489$ (top) and $N = 891$ (bottom) at $T = 100$ K after a simulated annealing procedure: (top left/right) top/side view for $N = 489$, (bottom left/right) top/side view for $N = 891$. The concave facets at the twin boundaries in the top left panel show that it is close to a Marks decahedron.

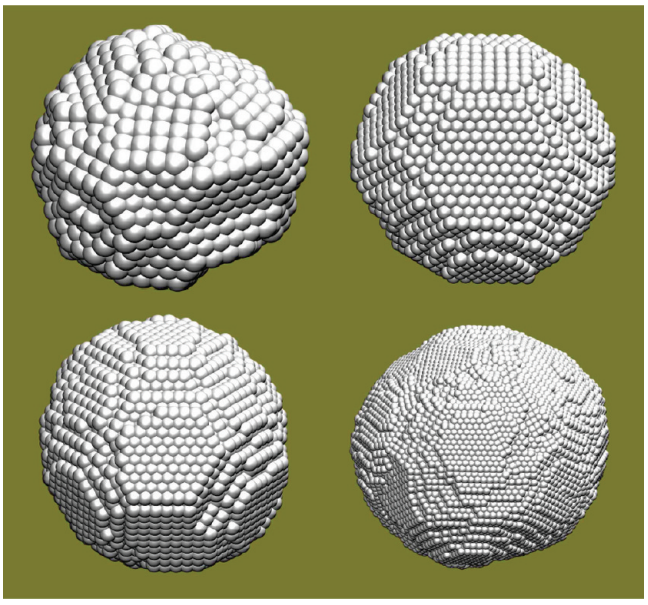

Figure 5. Structures of Ag nanoparticles obtained at $T = 100$ K after a simulated annealing procedure. (Top left) Irregular structure for $N = 2255$. (Top right) Truncated octahedral structure for $N = 6181$. (Bottom left) Truncated octahedral structure for $N = 8119$. (Bottom right) Irregular structure for $N = 45\,961$.

truncated decahedron and truncated octahedron. Decahedron and icosahedron are even higher, and tetrahedron is the highest.

For Au nanoparticles, as shown in the top panel of Figure 2, the minimized energy of icosahedron is the lowest in the size range $N < 500$. In the size range $500 < N < 2000$, the octahedron has the lowest energy. The minimized energies of truncated decahedral and truncated octahedral structures are also very low: that of decahedron is higher and tetrahedron has the highest. In the middle panel of Figure 2, the minimized energies of the truncated decahedral, truncated octahedral, and octahedral structures are almost the same and lower than the decahedral, icosahedral, and tetrahedral structures. In the bottom panel of Figure 2, in the region $10\,000 < N < 15\,000$, octahedron and truncated octahedron have similar energies and are the lowest. The truncated octahedron becomes the lowest at $N > 15\,000$. The minimized energy of octahedron is also very low. Those of decahedron and icosahedron are higher, and tetrahedron has the highest.

In Figure 2, minimized energies of octahedral and truncated octahedral structures are very close to each other, probably because the difference between the surface energy density coefficients of (111) and (100) Au surfaces calculated with the Sutton−Chen potential (0.549 J/m^2 for (111) surface, and 0.619 J/m^2 for (100) surface) are smaller than the experimental values, as seen in Table 1. From the minimization results shown in Figures 1 and 2, we can see a general trend that the icosahedral structure is the most stable in the smallest size regions, the truncated octahedral structure is the most stable in large size regions, and the truncated decahedral structure is the most stable in some intermediate size regions. This is qualitatively consistent with Marks' prediction[57,58] that the Marks truncated decahedron is most preferrable at an intermediate size region between icosahedron and truncated octahedron, as later confirmed by Baletto et al.,[59,60] despite our not studying the Marks truncated decahedron, which, in addition to the truncated decahedron, has concave facets at the twin boundaries.

Next we compare the minimized energies of the constructed perfect nanocrystals with those from the analytical calculations with Ino's theory. In the top and middle panels of Figure 1, for Ag nanoparticles with $N < 10\,000$, we can see that the minimized energies of all structures are very close to those calculated from Ino's theory, except that, for decahedral and tetrahedral structures, theoretical energies are higher than the minimized energies. In the bottom panel of Figure 1, for $N > 10\,000$, the minimized energies of all structures are very close to those calculated from Ino's theory, except that, for octahedral and truncated octahedral structures, theoretical energies are lower than the minimized energies. For Au naoparticles, for $N < 10\,000$ in the top and middle panels of Figure 2, the minimized energies of all structures are very close to those calculated from Ino's theory. In the bottom panel of Figure 2, the minimized energies of all structures are quite close to the energies calculated from Ino's theory, except for decahedral and truncated decahedral structures at larger sizes of $N > 14\,500$. The small deviations between the minimized energies and the analytical calculations in the large size regions might be due to the limitation of Ino's theory that edges and corners of nanoparticles are not included. Barnard's model has included energy terms for edges and corners of nanoparticles and showed that these terms are non-negligible.[61]

In order to compare between different force fields, the many-body glue potential for gold[81] was also used to perform the same calculations for Au nanoparticles. Various perfect structures of Au nanoparticles were manually generated and minimized. The results are plotted in Figure 3. We can see that the minimized energies obtained from the glue model are higher than those from the Sutton−Chen potential, and the calculated stability is also quite different. The minimized energies of decahedron,

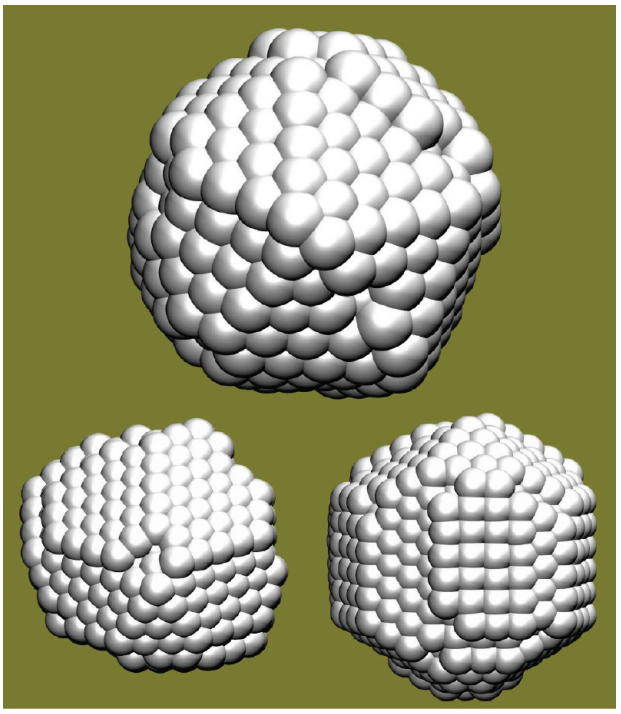

Figure 6. Structures of Au nanoparticles obtained at T = 100 K after a simulated annealing procedure. (Top) Icosahedral structure obtained for N = 489. (Bottom) Truncated decahedral structure obtained for N = 891. The concave facets in the top view (bottom left) and side view (bottom right) of the 891-atom cluster show that it is a Marks decahedron.

octahedron, and truncated octahedron are almost indistinguishable for $N < 2000$, and are lower than icosahedron, tetrahedron, and truncated decahedron. Octahedron becomes the lowest for $N > 2000$, but almost the same with truncated octaderon for N close to 50 000. Because the decreasing of the energy of truncated octahedron is faster than octahedron, it is very likely that truncated octahedron may have a lower energy than octahderon for $N > 50\,000$. The minimized energy of the tetrahedral structure is the highest at all sizes. The icosahedral structure is only slightly less stable than the decahedral structure for $N <$ 2000, and it becomes much less stable for larger N. An earlier simulated annealing result[76] has shown that all gold nanoclusters with N between 600 and 5000 stabilized in an icosahedral structure. This difference might be attributed to the thermodynamic effect incorporated in the simulated annealing procedure, as studied in the next section.

4. STRUCTURES OBTAINED BY SIMULATED ANNEALING

In experimental processes of metal nanoparticle growth, a thermodynamic effect is generally present, so the obtained structure is unnecessarily always the structure with the lowest potential energy. To evaluate the degree of thermodynamic effects, the simulated annealing method, categorized as one of the major global optimization methods,[77] was applied to Ag and Au nanoparticles with various sizes. The obtained stable structures at a very low temperature of T = 100 K were compared with those obtained from both Ino's theory and the energy minimization method. The simulated annealing simulations were

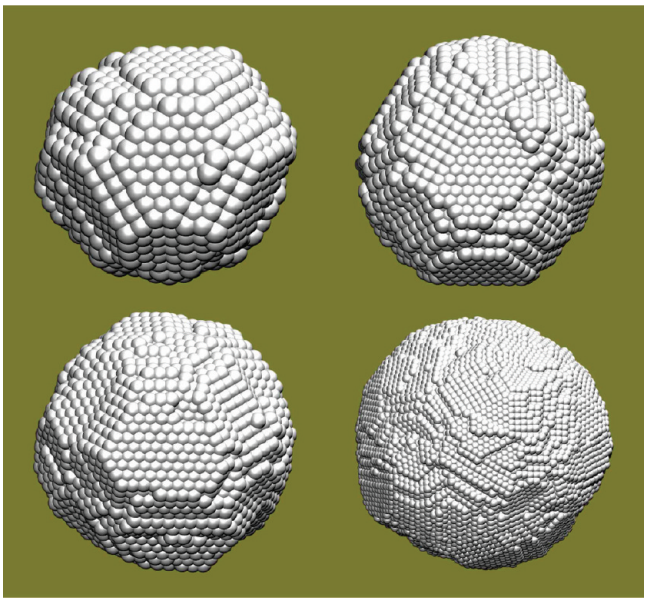

Figure 7. Structures of Au nanoparticles obtained at T = 100 K after a simulated annealing procedure. (Top left) Truncated octahedral structure for N = 2255. (Top right) Truncated octahedral structure obtained for N = 6181. (Bottom left) Irregular structure obtained for N = 8119. (Bottom right) Irregular structure for N = 45 961.

performed by the DL_POLY software package[82] with the Sutton−Chen many-body force field.[79] The Nosé−Hoover thermostat[83,84] with a relaxation constant of 0.1 ps was used to mimic the constant NVT ensemble.

The Ag and Au nanoparticles with various sizes were first equilibrated at a high temperature of T = 1200 K, when the nanoparticles are liquid, and then cooled down step by step with a temperature interval of 100 K until it reached a very low T = 100 K. At each temperature, a 20 ns MD simulation was performed for particles with $N < 2000$, 10 ns for $2000 < N <$ 10 000, and 4 ns for $N > 10\,000$. In Figures 4 and 5, we show the equilibrated structures of Ag nanoparticles with 489, 891, 2255, 6181, 8119, and 45961 atoms, respectively, at T = 100 K after the simulated annealing procedure. We have found that the 489-atom Ag nanoparticle (as shown in the top of Figure 4) has the Marks decahedron structure.[57,58] The 891-atom Ag nanoparticle has the truncated decahedron structure. The 2255-atom Ag nanoparticle has a structure with fragmented facets, as shown in the top left of Figure 5, possibly because it is in the transition region when the most stable structure changes from truncated decahedron to truncated octahedron. The Ag nanoparticles with 6181 and 8119 atoms were both stabilized with a truncated octahedral structure, seen in the top right and bottom left of Figure 5, which is consistent with Ino's theoretical predictions. The 45 961-atom Ag nanoparticle has an irregular shape close to a sphere, with fragmented (111) and (100) facets covering its surface, seen in the bottom right of Figure 5.

The Au nanoparticle with 489 atoms has an icosahedral structure after simulated annealing, as shown in the top of Figure 6. This is consistent with the theoretical prediction of Ino's theory and the energy minimization results shown in Figure 2. The 891-atom Au nanoparticle has a Marks decahedral structure, as shown in the bottom of Figure 6. The 2255-atom and 6181-atom Au nanoparticles have the truncated octahedral structure with some defects on the surface, seen in the top left

and top right of Figure 7. The 8119-atom Au nanoparticle has a fragmented surface structure, except that part of it has the truncated octahedral structure, as can be seen from its front view in the bottom left of Figure 7. The 45 961-atom Au nanoparticle has an irregular structure close to a sphere, covered by fragmented (111) and (100) facets, seen in the bottom right of Figure 7, because the simulation time in the simulated annealing procedure is too fast to allow the structure to better relax.

The average potential energies per atom of the nanoparticles at T = 100 K obtained from simulated annealing are plotted in Figures 1 and 2 as black stars. Due to thermodynamic effects, they are all slightly higher than the energies obtained from both Ino's theory and energy minimization. Those for the 45 961-atom Ag and Au nanoparticles are −2.852 eV and −3.718 eV, respectively, which are not plotted in the figures since they are out of the range of our plots.

5. CONCLUSIONS

Ino's theory was re-examined for Ag and Au nanoparticles by using the parameters determined from the numerical calculations with the Sutton−Chen empirical force field for silver and gold, respectively. Qualitatively agreeing with Ino's calculations, our continuous analytic calculations showed that the icosahedral structure is the most stable in the small size region, and the truncated octahedral structure is the most stable in the large size region. However, in our calculations, the structural transition happens at a smaller diameter of about 2 nm rather than 10 nm in Ino's original calculations.[56]

Static energies for perfect crystalline structures were then calculated to evaluate the errors in Ino's theory, caused by the assumptions made in the composition and continuous change with size of the internal energy. It was found that, for Ag with the Sutton−Chen force field, the icosahedral structure is the most stable in the small size region, the truncated decahedral structure is the most stable in an intermediate size region, and the truncated octahedral structure is the most stable in the large size region. For Au with Sutton−Chen force field, the icosahedral structure is the most stable in the small size region and the octahedral structure is the most stable in an intermediate region of small sizes. The truncated decahedral, truncated octahedral, and octahedral structures are almost all the most stable in an intermediate region of larger sizes. The octahedron and truncated octahedron have similar energies and are both the most stable in the next intermediate size region, and the truncated octahedron is the most stable in the large size region. For Au with the glue model, decahedron, octahedron, and truncated octahedron are almost all the most stable in the small size region, and the octahedron is the most stable in the large size region, but truncated octahedron is likely to become the most stable at $N >$ 50 000. The static energy calculations indicate that the analytical calculations can not capture the delicacy of nanoparticles, because the continuous assumption does not work well when the system size is small. However, analytical calculations indicate that both Au and Ag clusters adopt a truncated octahedral structure when the system size is large enough, which is supported by the static energy calculations. It should be noted that more complete studies have been done for the structural motifs of very small nanoparticles, such as those reported in refs 60 and 85−87, but they are not the central focus of this paper.

The influence of thermodynamic effects was evaluated by the MD simulations with the simulated annealing method. The structures given by the simulated annealing method were not always those with the lowest energy, consistent with the molecular dynamics simulation results of the freezing of silver[88] and gold[89] nanoclusters. Therefore, the thermodynamic effect is non-negligible and should be in count when studying the structures of experimentally constructed metal nanoparticles.

AUTHOR INFORMATION

Corresponding Author

*E-mail: wangyt@itp.ac.cn.

ACKNOWLEDGMENT

This work was supported by the Hundred Talent Program of the Chinese Academy of Sciences and the National Natural Science Foundation of China under Grant 10835005. Allocations of computer time from the Supercomputing Center in the Computer Network Information Center at the Chinese Academy of Sciences are gratefully acknowledged.

REFERENCES

(1) Ahmadi, T. S.; Wang, Z. L.; Green, T. C.; Henglein, A.; El-Sayed, M. A. *Science* **1996**, *272*, 1924–1926.
(2) Peng, X. G.; Manna, L.; Yang, W. D.; Wickham, J.; Scher, E.; Kadavanich, A.; Alivisatos, A. P. *Nature* **2000**, *404*, 59–61.
(3) Cui, Y.; Lieber, C. M. *Science* **2001**, *291*, 851–853.
(4) Iijima, S. *Nature* **1991**, *354*, 56–58.
(5) Murray, C. B.; Sun, S. H.; Doyle, H.; Betley, T. *MRS Bull.* **2001**, *26*, 985–991.
(6) O'Brien, S.; Brus, L.; Murray, C. B. *J. Am. Chem. Soc.* **2001**, *123*, 12085–12086.
(7) Campbell, C. T. *Science* **2004**, *306*, 234–235.
(8) Medintz, I. L.; Uyeda, H. T.; Goldman, E. R.; Mattoussi, H. *Nat. Mater.* **2005**, *4*, 435–446.
(9) Akin, D.; Sturgis, J.; Ragheb, K.; Sherman, D.; Burkholder, K.; Robinson, J. P.; Bhunia, A. K.; Mohammed, S.; Bashir, R. *Nat. Nanotechnol.* **2007**, *2*, 441–449.
(10) Li, J.; Gong, X.; Lu, H.; Li, D.; Fang, H.; Zhou, R. *Proc. Natl. Acad. Sci. U.S.A.* **2007**, *104*, 3687–3692.
(11) Wang, B.; Král, P. *Phys. Rev. Lett.* **2007**, *98*, 266102.
(12) Wang, B.; Vuković, L.; Král, P. *Phys. Rev. Lett.* **2008**, *101*, 186808.
(13) Valden, M.; Lai, X.; Goodman, D. W. *Science* **1998**, *281*, 1647–1650.
(14) Haruta, M. *Catal. Today* **1997**, *36*, 153–166.
(15) Wynblatt, P.; Gjostein, N. A. In *Progress in Solid State Chemistry*; McCaldin, J. O., Somorjai, G. A., Eds.; Elsevier Science: Amsterdam, 1975; pp 21−58.
(16) Wynblatt, P.; Gjostein, N. A. *Acta Metall.* **1976**, *24*, 1165–1174.
(17) Ruckenstein, E.; Dadyburjor, D. B. *Rev. Chem. Eng.* **1983**, *1*, 251–261.
(18) Bartholomew, C. H.; Fuentes, G. A. *Catalyst Deactivation*; Elsevier Science: Amsterdam, 1997.
(19) Campbell, C. T. *Surf. Sci. Rep.* **1997**, *27*, 1–111.
(20) Jang, M.; Czoschke, N. M.; Lee, S.; Kamens, R. M. *Science* **2002**, *298*, 814–817.
(21) Ridley, B. A.; Nivi, B.; Jacobson, J. M. *Science* **1999**, *286*, 746–749.
(22) Morgan, N. Y.; Leatherdale, C. A.; Jarosz, M. V.; Drndić, M.; Kastner, M. A.; Bawendi, M. *Phys. Rev. B* **2002**, *66*, 075339.
(23) Yu, D.; Wang, C.; Guyot-Sionnest, P. *Science* **2003**, *300*, 1277–1280.
(24) Talapin, D. V.; Murray, C. B. *Science* **2005**, *310*, 86–89.
(25) Kim, H.; Cho, K.; Kim, D.-W.; Lee, H.-R.; Kim, S. *Appl. Phys. Lett.* **2006**, *89*, 173107.

(26) Porter, V. J.; Mentzel, T.; Charpentier, S.; Kastner, M. A.; Bawendi, M. G. *Phys. Rev. B* **2006**, *73*, 155303.
(27) Urban, J. J.; Talapin, D. V.; Shevchenko, E. V.; Kagan, C. R.; Murray, C. B. *Nat. Mater.* **2007**, *6*, 115–121.
(28) Ginger, D. S.; Greenham, N. C. *J. Appl. Phys.* **2000**, *87*, 1361–1368.
(29) Jarosz, M. V.; Porter, V. J.; Fisher, B. R.; Kastner, M. A.; Bawendi, M. G. *Phys. Rev. B* **2004**, *70*, 195327.
(30) Oertel, D. C.; Bawendi, M. G.; Arango, A. C.; Bulović, V. *Appl. Phys. Lett.* **2005**, *87*, 213505.
(31) Konstantatos, G.; Howard, I.; Fischer, A.; Hoogland, S.; Clifford, J.; Klem, E.; Levina, L. E.; Sargent, E. H. *Nature* **2006**, *442*, 180–183.
(32) Colvin, V. L.; Schlamp, M. C.; Alivisatos, A. P. *Nature* **1994**, *370*, 354–357.
(33) Artemyev, M. V.; Sperling, V.; Woggon, U. *J. Appl. Phys.* **1997**, *81*, 6975–6977.
(34) Gao, M.; Lesser, C.; Kirstein, S.; Möhwald, H.; Rogach, A. L.; Weller, H. *J. Appl. Phys.* **2000**, *87*, 2297–2302.
(35) Coe, S.; Woo, W.-K.; Bawendi, M.; Bulović, V. *Nature* **2002**, *420*, 800–803.
(36) Bertoni, C.; Gallardo, D.; Dunn, S.; Gaponik, N.; Eychmüller, A. *Appl. Phys. Lett.* **2007**, *90*, 034107.
(37) Redl, F. X.; Cho, K.-S.; Murray, C. B.; O'Brien, S. *Nature* **2003**, *423*, 968–971.
(38) Shevchenko, E. V.; Talapin, D. V.; Kotov, N. A.; O'Brien, S.; Murray, C. B. *Nature* **2006**, *439*, 55–59.
(39) Shevchenko, E. V.; Talapin, D. V.; Murray, C. B.; O'Brien, S. *J. Am. Chem. Soc.* **2006**, *128*, 3620–3637.
(40) Nozik, A. J. *Physica E* **2002**, *14*, 115–120.
(41) Gur, I.; Fromer, N. A.; Geier, M. L.; Alivisatos, A. P. *Science* **2005**, *310*, 462–465.
(42) Hamdoun, B.; Ausserre, D.; Joly, S.; Gallot, Y.; Cabuil, V.; Clinard, C. *J. Phys. II* **1996**, *6*, 493–501.
(43) Hamdoun, B.; Ausserre, D.; Cabuil, V.; Joly, S. *J. Phys. II* **1996**, *6*, 503–510.
(44) Lo, C.-T.; Lee, B.; Pol, V. G.; Dietz Rago, N. L.; Seifert, S.; Winans, R. E.; Thiyagarajan, P. *Macromolecules* **2007**, *40*, 8302–8310.
(45) Bockstaller, M. R.; Thomas, E. L. *Phys. Rev. Lett.* **2004**, *93*, 166106.
(46) Chiu, J. J.; Kim, B. J.; Kramer, E. J.; Pine, D. J. *J. Am. Chem. Soc.* **2005**, *127*, 5036–5037.
(47) Kang, H.; Detcheverry, F. A.; Mangham, A. N.; Stoykovich, M. P.; Daoulas, K. C.; Hamers, R. J.; Muller, M.; dePablo, J. J.; Nealey, P. F. *Phys. Rev. Lett.* **2008**, *100*, 148303.
(48) Oh, H.; Green, P. F. *Nat. Mater.* **2009**, *8*, 139–143.
(49) Koparde, V. N.; Cummings, P. T. *ACS Nano* **2008**, *2*, 1620–1624.
(50) Law, M.; Luther, J. M.; Song, Q.; Hughes, B. K.; Perkins, C. L.; Nozik, A. J. *J. Am. Chem. Soc.* **2008**, *130*, 5974–5985.
(51) Tsyganov, S.; Kästner, J.; Rellinghaus, B.; Kauffeldt, T.; Westerhoff, F.; Wolf, D. *Phys. Rev. B* **2007**, *75*, 045421.
(52) Bezemer, G. L.; Remans, T. J.; van Bavel, A. P.; Dugulan, A. L. *J. Am. Chem. Soc.* **2010**, *132*, 8540–8541.
(53) Campbell, C. T.; Parker, S. C.; Starr, D. E. *Science* **2002**, *298*, 811–814.
(54) Brown, M. A.; Carrasco, E.; Sterrer, M.; Freund, H.-J. *J. Am. Chem. Soc.* **2010**, *132*, 4064–4065.
(55) Wulff, G. Z. *Kristallogr. Mineral.* **1901**, *34*, 449–530.
(56) Ino, S. *J. Phys. Soc. Jpn.* **1969**, *27*, 941–953.
(57) Marks, L. D. *J. Cryst. Growth* **1983**, *61*, 556–566.
(58) Marks, L. D. *Rep. Prog. Phys.* **1994**, *57*, 603–649.
(59) Baletto, F.; Ferrando, R. *Rev. Mod. Phys.* **2005**, *77*, 371–423.
(60) Baletto, F.; Ferrando, R.; Fortunelli, A.; Montalenti, F.; Mottet, C. *J. Chem. Phys.* **2002**, *116*, 3856–3863.
(61) Barnard, A. S. *J. Phys. Chem. B* **2006**, *110*, 24498–24504.
(62) Barnard, A. S.; Zapol, P. *J. Chem. Phys.* **2004**, *121*, 4276–4283.
(63) Barnard, A. S.; Curtiss, L. A. *ChemPhysChem* **2006**, *7*, 1544–1553.
(64) Harberlen, O. D.; Chung, S.-C.; Stener, M.; Rosch, N. *J. Chem. Phys.* **1997**, *106*, 5189–5201.
(65) Hakkinen, H.; Landman, U. *Phys. Rev. B* **2000**, *62*, 2287–2290.
(66) Wang, J. L.; Wang, G. H.; Zhao, J. J. *Phys. Rev. B* **2002**, *66*, 035418.
(67) Oviedo, J.; Palmer, R. E. *J. Chem. Phys.* **2002**, *117*, 9548–9551.
(68) Gilb, S.; Weis, P.; Furche, F.; Ahlrichs, R.; Kappes, M. M. *J. Chem. Phys.* **2002**, *116*, 4094–4101.
(69) Zhao, J.; Yang, J.; Hou, J. G. *Phys. Rev. B* **2003**, *67*, 085404.
(70) Hakkinen, H.; Moseler, M. *Comput. Mater. Sci.* **2006**, *35*, 332–336.
(71) Cleveland, C. L.; Landman, U.; Schaaff, T. G.; Shafigullin, M. N.; Stephens, P. W.; Whetten, R. L. *Phys. Rev. Lett.* **1997**, *79*, 1873–1876.
(72) Cleveland, C. L.; Luedtke, W. D.; Landman, U. *Phys. Rev. Lett.* **1998**, *81*, 2036–2039.
(73) Garzón, I. L.; Michaelian, K.; Beltrán, M. R.; Posada-Amarillas, A.; Ordejón, P.; Artacho, E.; Sánchez-Portal, D.; Soler, J. M. *Phys. Rev. Lett.* **1998**, *81*, 1600–1603.
(74) Cleveland, C. L.; Luedtke, W. D.; Landman, U. *Phys. Rev. B* **1999**, *60*, 5065–5077.
(75) Nam, H. S.; Hwang, N. M.; Yu, B. D.; Yoon, J. K. *Phys. Rev. Lett.* **2002**, *89*, 275502.
(76) Wang, Y.; Teitel, S.; Dellago, C. *J. Chem. Phys.* **2005**, *122*, 214722–214738.
(77) Barnard, A. S. *Rep. Prog. Phys.* **2010**, *73*, 086502.
(78) Allen, M. P.; Tildesley, D. J. *Computer Simulation of Liquids*; Oxford University Press: New York, 1987.
(79) Sutton, A. P.; Chen, J. *Philos. Mag. Lett.* **1990**, *61*, 139–164.
(80) Daw, M. S.; Baskes, M. I. *Phys. Rev. B* **1984**, *29*, 6443–6453.
(81) Ercolessi, F; Parrinello, M.; Tosatti, E. *Philos. Mag. A* **1988**, *58*, 213–226.
(82) Forester, T. R.; Smith, W. *DL-POLY User Manual*; CCLRC, Daresbury Laboratory: Daresbury, U.K., 1995.
(83) Nosé, S. *J. Chem. Phys.* **1984**, *81*, 511–519.
(84) Hoover, W. G. *Phys. Rev. A* **1985**, *31*, 1695–1697.
(85) Angulo, A. M.; Noguez, C. *J. Phys. Chem. A* **2008**, *112*, 5834–5838.
(86) Yang, X.; Cai, W.; Shao, X. *J. Phys. Chem. A* **2007**, *111*, 5048–5056.
(87) Michaelian, K.; Rendón, N.; Garzón, I. L. *Phys. Rev. B* **1999**, *60*, 2000–2010.
(88) Baletto, F.; Mottet, C.; Ferrando, R. *Chem. Phys. Lett.* **2002**, *354*, 82–87.
(89) Rossi, G.; Ferrando, R. *Nanotechnology* **2007**, *18*, 225706 (6).